Applied Physics Letters

A comprehensive study of charge transport in Au-contacted graphene on Ge/Si(001)

Cite as: Appl. Phys. Lett. **117**, 023104 (2020); https://doi.org/10.1063/5.0013802
Submitted: 14 May 2020 . Accepted: 01 July 2020 . Published Online: 15 July 2020

Anna Sinterhauf, Simeon Bode, Manuel Auge, Mindaugas Lukosius, Gunther Lippert, Hans-Christian Hofsäss, and Martin Wenderoth

Applied Physics Letters ARTICLE scitation.org/journal/apl

A comprehensive study of charge transport in Au-contacted graphene on Ge/Si(001)

Cite as: Appl. Phys. Lett. **117**, 023104 (2020); doi: 10.1063/5.0013802
Submitted: 14 May 2020 · Accepted: 1 July 2020 ·
Published Online: 15 July 2020

Anna Sinterhauf,[1,a)] Simeon Bode,[1] Manuel Auge,[2] Mindaugas Lukosius,[3] Gunther Lippert,[3] Hans-Christian Hofsäss,[2] and Martin Wenderoth[1,a)]

AFFILIATIONS

[1]IV. Physikalisches Institut, Georg-August-Universität Göttingen, Friedrich-Hund-Platz 1, 37077 Göttingen, Germany
[2]II. Physikalisches Institut, Georg-August-Universität Göttingen, Friedrich-Hund-Platz 1, 37077 Göttingen, Germany
[3]IHP–Leibniz-Institut für innovative Mikroelektronik, Im Technologiepark 25, 15236 Frankfurt (Oder), Germany

[a)]**Authors to whom correspondence should be addressed:** anna.sinterhauf@uni-goettingen.de and martin.wenderoth@uni-goettingen.de

ABSTRACT

We investigate the electronic transport properties of Au-contacted graphene on Ge/Si(001). Kelvin probe force microscopy at room temperature with an additionally applied electric transport field is used to gain a comprehensive understanding of macroscopic transport measurements. In particular, we analyze the contact pads including the transition region, perform local transport measurements in pristine graphene/Germanium, and explore the role of the semiconducting Germanium substrate. We connect the results from these local scale measurements with the macroscopic performance of the device. We find that a graphene sheet on a 2 μm Ge film carries approximately 10% of the current flowing through the device. Moreover, we show that an electronic transition region forms directly adjacent to the contact pads. This transition region is characterized by a width of >100 μm and a strongly increased sheet resistance acting as the bottleneck for charge transport. Based on Rutherford backscattering of the contact pads, we suggest that the formation of this transition region is caused by diffusion.

The successful growth of large-scale graphene on Ge/Si(001)[1] has been a significant step toward the integration of graphene into silicon-based device technologies.[2] To this end, several studies have focused on the performance of graphene on Germanium (Gr/Ge) devices.[3,4] However, all experimental approaches to access transport properties so far have been done using conventional macroscopic transport geometries. To improve the transport properties of a device, it is crucial to understand drawbacks and limitations on the local scale, i.e., to explore where exactly voltage drops occur. This question can only be addressed by locally resolved transport measurements. This knowledge on a scale well below the micrometer scale is the basis for the development of targeted strategies to improve the overall performance of a given device. Scanning probe techniques have shown to be a versatile method to characterize charge transport down to this scale[5] as demonstrated for transport properties of graphene on SiC dominated by atomic scale defects[6–8] or the proximity to the substrate.[9] Combining Kelvin probe force microscopy (KPFM) with an electric transport field across the sample has given access to charge transport under realistic device conditions bridging the local scale and the μm-scale.[10] In this study, we contrast KPFM with macroscopic transport measurements to comprehensively investigate charge transport in Au-contacted Gr/Ge/Si(001).

We have analyzed a Gr/Ge/Si(001) device with a width of 1.4 mm and a length of 1.8 mm contacted in a two-terminal geometry [Fig. 1(a)]. Graphene was grown by chemical vapor deposition (CVD) on 200 mm Si(001) wafers. In a first step, a 2 μm thick Germanium layer was deposited onto the silicon substrate by CVD.[11] Despite the absence of a dopant source during the Ge growth process, the epitaxial Ge layer exhibits a light doping of $<1 \times 10^{15}/\mathrm{cm}^3$. The graphene growth was initialized in a 700 mbar Ar/H_2 environment at a deposition temperature of 885 °C using CH_4 as the carbon source. The deposition time was 60 min.[1] The homogeneity of the graphene layer over the area of the 200 mm Si(001) wafer was verified by Raman mapping (see the supplementary material, Fig. S1). Then, the wafer was cut into smaller rectangular pieces and contact pads (film thickness ≈35 nm) were deposited by a shadow mask procedure using thermal evaporation of Au in high vacuum (5×10^{-7} mbar). The contact pads were electrically connected using Aluminum wire bonds. The measurements

presented here were obtained from a single device that we analyzed in great detail from left to right, i.e., from contact to contact. To ensure reproducibility, a total of nine devices were manufactured on which different aspects of the measurements presented in this study were tested. All devices showed qualitatively consistent results.

In a first step, we analyze the surface morphology of our device. We carried out topographic imaging using a commercial AFM setup (Agilent 5600LS) operated in tapping mode. We separate three distinct surface regions with different surface morphologies (Fig. 1): first, pristine Gr/Ge, second, the contact pads, and third, the transition from the contact pads to graphene. (i) The surface structure of pristine Gr/Ge(001) is dominated by facets oriented 90° to each other with a facet height of approximately 4 nm [Fig. 1(b)]. The faceting of the surface occurs during the graphene growth process.[3] Surface step pinning at graphene nuclei breaks up the surface into (107) facets under the sublimation of Ge atoms.[1] (ii) AFM topographies of the contact pads [Figs. 1(e)–1(g)] reveal a height of approximately 35 nm. Moreover, the contact pads [Fig. 1(c)] show an inhomogeneous surface morphology with round holes (Fig. 1). With the used tip geometry (tip height 17 μm, tip radius at the apex 10 nm, and half cone angle ≈25°), we find a depth of up to 80 nm with a diameter of less than 3 μm [Fig. 1(d)]. Hence, the depth of the holes significantly extends the thickness of the contact pads. The presence of such holes can indicate diffusion processes that can lead to the formation of diffusion channels in the form of micropipes or voids.[12] (iii) Topographies across the contact edges additionally provide insight into the surface morphology of areas adjacent to the contact pads. For the Au/Graphene contact on SiC, one finds a nearly abrupt interface.[13] In contrast for this device, the areas adjacent to the contact pads show structural similarities with the morphology of the contact pads. In particular, here, we also find round holes [Figs. 1(e) and 1(f)].

As the AFM results indicate a diffusion process, we employ Rutherford backscattering (RBS) to determine the chemical composition of the contact pads. In Fig. 2, we compare the RBS spectrum of pristine Gr/Ge/Si(001) with that of Au-contacted Gr/Ge/Si(001). The signal at ion energies of (725–800) keV reflects the thin film on top of Gr/Ge. Besides the presence of the Au-related peak, the RBS spectrum of Au-contacted Gr/Ge/Si(001) reveals a depletion at energies around

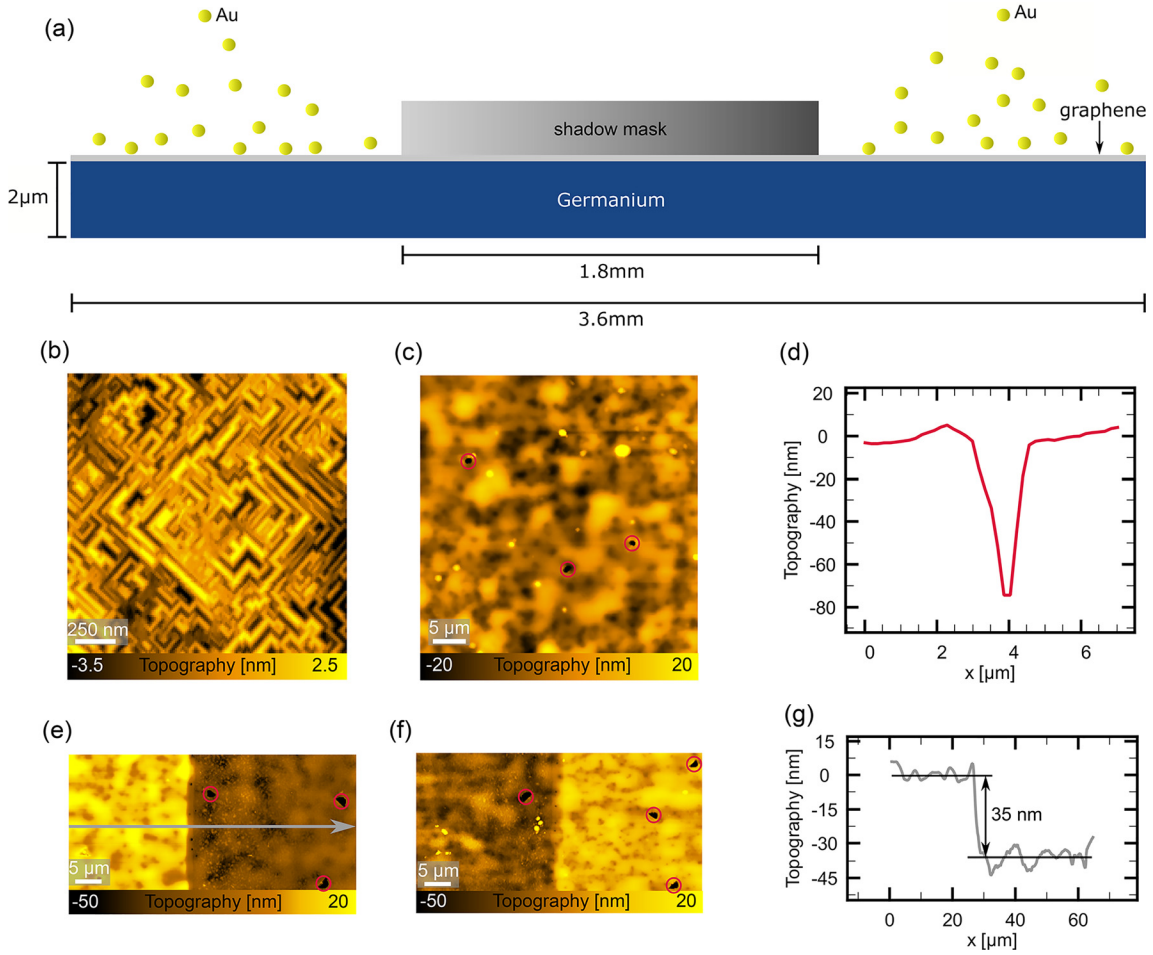

FIG. 1. (a) Au contact pads of 35 nm thickness are deposited onto Gr/Ge/Si(001). (b) AFM topography of pristine Gr/Ge/Si(001). (c) AFM topography of the contact and (d) line profile across one of the holes marked in (c). AFM topographies across the left (e) and right (f) contact edge and (g) line profile along the gray arrow in (e).

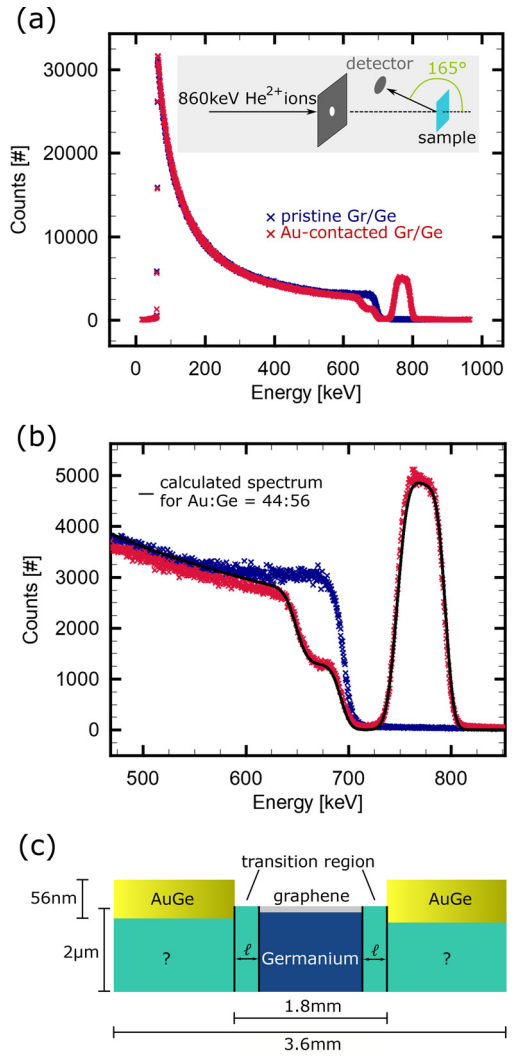

FIG. 2. RBS analysis of the contact pads: 860 keV He^{2+} ions are accelerated toward the sample (inset). The graphene monolayer is not visible. (a) RBS spectra of pristine Gr/Ge/Si(001) (not contacted) and for Au-contacted Gr/Ge/Si(001). (b) Close-up highlighting the prominent features of the RBS spectra and the best fit. (c) Side view of the "realistic" Gr/Ge/Si(001) device. The thickness is depicted in a not-to-scale manner.

675 keV. For a quantitative analysis of the RBS data, we use the software package SIMNRA.[14] Both features, the peak and the depletion, can be modeled using an AuGe alloy for the contact pads instead of a pure Au film. The best fit to the experimental spectrum is achieved with an AuGe ratio of 44:56 [Fig. 2(b)]. In addition, the thickness of the AuGe film can be determined by analyzing the FWHM of the peak in the energy range of (725–800)keV. We find a thickness of (56 ± 3)nm. This value is significantly larger than the topographic height of the contact pads of ≈35 nm [Figs. 1(e)–1(g)]. Summarizing the RBS result, a strong interdiffusion of Au and Ge is present in our sample, which has to be considered while analyzing the transport properties.

In a first step, we have performed standard macroscopic current–voltage measurements. The resulting I(V) relation of the entire device exhibits a linear behavior in the investigated voltage range of ±5 V [Fig. 3(b)]. We calculate the overall macroscopic sheet resistance (approximating charge transport in our device by a 2D transport geometry) extracting a value of $\rho^{\square}_{\text{macro}} = (110 \pm 1)\,\frac{\Omega}{\square}$ [Fig. 3(b)]. As the contact pads reach into the Ge bulk [Fig. 2(c)] and, thus, directly come into contact with the Ge film electrically, the device exhibits two parallel conduction channels, the graphene layer and the Ge film. In order to disentangle the contributions of these two conducting channels, we exfoliated the graphene layer using the Scotch tape technique. The removal of the graphene layer is confirmed by work function measurements using conventional KPFM (supplementary material Fig. S2). The macroscopic I(V) curve shows an increased resistance by approximately 10% [Fig. 3(b)]. The linear behavior is an indication of Ohmic contact to Germanium.

To disentangle local scale contributions from different parts of our device to the overall macroscopic resistance, we make use of KPFM. The advantage of using KPFM in comparison to the conventional transmission line method for determining sheet and contact resistances is that KPFM measures the evolution of the voltage drop with the spatial resolution of the AFM and, thus, gives access to local charge transport phenomena. KPFM measurements were performed in frequency modulation KPFM mode under ambient conditions in a two-terminal geometry [Fig. 3(a)]. For all KPFM measurements, we used Si tips with a 5 nm/20 nm Ti/Pt coating and a tip apex radius of <25 nm. The tips were excited to oscillate near their resonance frequency of 70 kHz. In order to avoid temperature-dependent effects due to Joule heating,[10] the samples were mounted on a Cu plate during KPFM measurements.

In Fig. 3(c), the transport signal in pristine Gr/Ge is shown, and the simultaneously acquired topography is given in supplementary material Fig. S3(a). We extract the averaged voltage drop along the x-direction (parallel to the macroscopic current flow direction), as shown in Fig. 3(d). From this, the local sheet resistance $\rho^{\square} = \frac{\frac{\partial V}{\partial x}}{j_{\text{macro}}} = \frac{E_x}{j_{\text{macro}}}$ can be calculated, where j_{macro} is the macroscopic 2D current density determined from the I(V) characteristics and the sample geometry. We find a sheet resistance of $\rho^{\square}_{\text{Gr/Ge}} = (66 \pm 2)\,\frac{\Omega}{\square}$ (Table I), which is in the same order of magnitude as room temperature Hall bar measurements of Gr/Ge.[4]

In order to separate the sheet resistance of the graphene sheet from the Germanium layer, we have performed KPFM measurements on exfoliated devices [Figs. 3(e) and 3(f), the simultaneously acquired topography is shown in supplementary material Fig. S3(b)]. We find a sheet resistance of the Germanium film of $\rho^{\square}_{\text{Ge}} = (77 \pm 5)\,\frac{\Omega}{\square}$ (Table I). Assuming that the current flow through the combined graphene-on-Germanium system can be described by a parallel circuit, we calculate the sheet resistance of graphene from $\rho^{\square}_{\text{Ge}}$ and $\rho^{\square}_{\text{Gr/Ge}}$ using $\rho^{\square}_{\text{Gr}} = \left(\frac{1}{\rho^{\square}_{\text{Gr/Ge}}} - \frac{1}{\rho^{\square}_{\text{Ge}}}\right)^{-1}$. This yields an estimation for the graphene layer of $\rho^{\square}_{\text{Gr}} = (460 \pm 120)\,\frac{\Omega}{\square}$. This value is comparable to the sheet resistance of high quality graphene on SiC at room temperature.[9] A direct comparison with published results is difficult because the sheet resistance of graphene grown on Ge substrates is usually measured on transferred samples, i.e., the graphene layer is transferred from the Ge/Si substrate onto a SiO_2/Si substrate,[1] or the measurements are

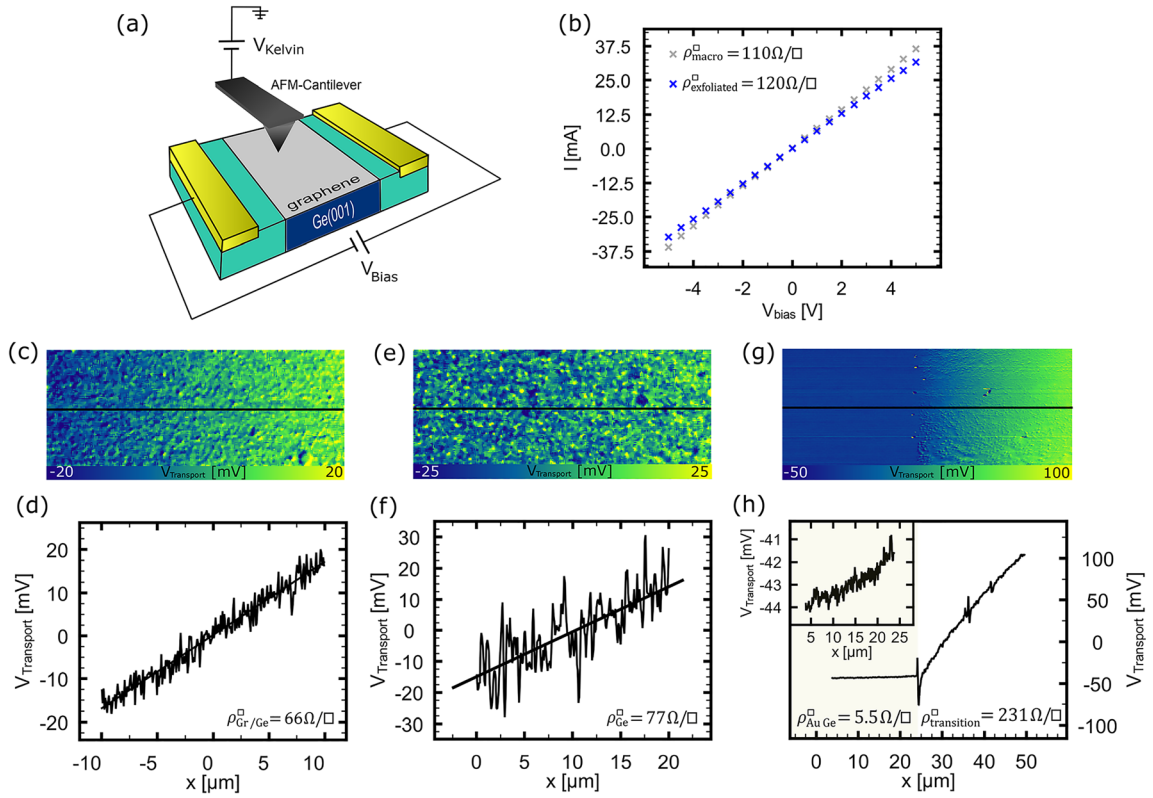

FIG. 3. (a) Schematics of the experimental setup, Gr/Ge/Si(001) contacted in a two-terminal geometry. (b) Macroscopic current–voltage relation for the Gr/Ge/Si(001) device and for the one conduction channel (graphene sheet removed by exfoliation). (c) $V_{Transport}$ for pristine Gr/Ge/Si(001) ($j_{macro} = 26.0\,Am^{-1}$) and (d) line profile along the black line in (c) representing the voltage drop parallel to the macroscopic current flow direction. (e) $V_{Transport}$ for Ge/Si(001) ($j_{macro} = 18.8\,Am^{-1}$) and (f) line profile along the black line in (e). (g) $V_{Transport}$ across the contact edge ($j_{macro} = 20.4\,Am^{-1}$) and (h) line profile along the black line in (g). The shaded area indicates the contact pad; the inset shows a close-up of the voltage drop in the contact.

performed at low temperatures to freeze the Ge conductivity.[3] A difference in the sheet resistance can, thus, be explained by residues of the transfer process and in the second case by an (up until now unknown) influence of the temperature. In addition, the pronounced diffusion of Au and Ge can affect the charge transport properties of our device and, thus, might also cause a deviation from published results.

Comparing a fictitious, averaged macroscopic sheet resistance $\rho^{\square}_{macro} = (110 \pm 1)\,\frac{\Omega}{\square}$, i.e., the resistivity of the entire device, with the local sheet resistance of Gr/Ge $\rho^{\square}_{Gr/Ge} = (66 \pm 2)\,\frac{\Omega}{\square}$, the macroscopic measurement is a factor of 1.8 larger than the local sheet resistance, indicating a significant "contact resistivity." To localize this contribution, we have analyzed the transport properties of the contact pads as well as the interface region between the contact pads and pristine Gr/Ge. A KPFM transport map across the contact edge is shown in Fig. 3(g), and the simultaneously acquired topography is given in supplementary material Fig. S3(c). While at the topographic contact edge, no significant jump in the potential is observed, the averaged voltage drop [Fig. 3(h)] reveals two clearly distinct slopes of the potential for both the contact pad and in the vicinity of the contact pad. Surprisingly, even the contact pad itself shows a non-vanishing voltage drop [Fig. 3(h)] with a sheet resistance of $5.5\,\frac{\Omega}{\square}$. Taking the RBS measurements into account, we attribute this significant and non-vanishing voltage drop in the contact region to a not perfectly metallic AuGe alloy.

Moreover, in the vicinity of the contact pad, a steep voltage slope is observed. The corresponding sheet resistance of $(231 \pm 11)\,\frac{\Omega}{\square}$ is larger than the sheet resistance of the Ge film (compare Table I). Obviously, the assumption of a parallel circuit does not hold in this

TABLE I. Sheet resistances of the different regions of the Au-contacted Gr/Ge/Si(001) device.

Sample region	$\rho\ \left[\frac{\Omega}{\square}\right]$	Method
Macro	110 ± 1	I(V)
Macro exfoliated	120 ± 1	I(V)
Pristine (Gr/Ge)	66 ± 2	KPFM
Exfoliated (Ge)	77 ± 5	KPFM
Contact region	5.5 ± 0.1	KPFM
Transition region	231 ± 11	KPFM
Gr	460 ± 120	Calculated

region. Instead, our results suggest that an extended transition region [schematically shown in Fig. 2(c)] is present in our sample exhibiting an increased sheet resistance compared to the contact pads and to the pristine Gr/Ge. As the width ℓ of this region [Fig. 2(c)] is beyond the scan range of our AFM, we estimate it using finite element simulations. As input parameters, the geometry of the investigated device and the measured resistances for the different regions are used. For the calculations, we model the transition region along both contact edges with a constant sheet resistance. Thus, the results yield a lower limit for the actual width of the transition region. For our device geometry, we find a minimum width of $\ell \approx 155\,\mu$m, which is approximately 9% of the total distance between the contact pads, i.e., large parts of our electronic device degenerate. Compared to the sheet resistance of pristine Gr/Ge, the transition region exhibits a 3.5× increased local sheet resistance (compare Table I). In conclusion, due to its large sheet resistance and its spatial extension, we identify the transition region as the bottleneck for charge transport in the investigated device. Moreover, this finding rationalizes the discrepancy between the macroscopically $\left[\rho^{\square}_{\mathrm{macro}} = (110 \pm 1)\,\frac{\Omega}{\square}\right]$ and the microscopically $\left[\rho^{\square}_{\mathrm{Gr/Ge}} = (66 \pm 2)\,\frac{\Omega}{\square}\right]$ determined sheet resistances.

From the results of our study, we conclude that diffusions play a crucial role in the investigated device. It leads to an entire intermixing of the Au film with Ge and causes the degeneration of the device in the vicinity of the contact pads. Based on the equilibrium phase diagram of the Au–Ge-system,[15] these findings are surprising. At equilibrium, the solid solubility of Au in Ge is negligible.[15] Furthermore, it is known from experimental studies that even at elevated temperatures (800 K–1100 K), Au in Ge exhibits only a relatively slow diffusivity.[16] Based on this, we propose a catalytic effect of the graphene sheet on the diffusion process. It has been shown experimentally[17] and confirmed by calculations[18] that Au atoms can diffuse in graphene. Au-doped graphene is predicted to be a very good electrocatalyst for oxygen reduction.[19] For the presented device, these electrocatalytic properties may directly affect the Ge oxide present at the Ge-graphene interface. Further investigations have to show how these diffusion processes affect the charge transport properties.

In summary, we have analyzed charge transport in Gr/Ge/Si(001) devices using a combination of macroscopic measurements and a local scale approach based on KPFM upgraded with an additionally applied electric transport field. We have found that at room temperature, the graphene sheet on 2 μm Ge carries approximately 10% of the current injected into the device. Furthermore, we have estimated the sheet resistance of the graphene layer at room temperature to $\approx 460\,\frac{\Omega}{\square}$. In addition, we have shown that for the investigated device design, an electronic transition region forms close to the contact edges. This transition region exhibits a strongly increased sheet resistance compared to pristine Gr/Ge. We propose that the degeneration of the device is driven by diffusion, resulting in AuGe alloy contacts and an extended transition region of $>100\,\mu$m. We have identified the consequences of this surprising strong diffusion process as the main limitations for charge transport in the examined device.

See the supplementary material for Raman measurements on pristine graphene on Ge/Si(001), work function differences for pristine graphene compared to the exfoliated device determined by conventional KPFM, and the simultaneously acquired topographies for the KPFM data shown in Fig. 3.

Financial support of the Deutsche Forschungsgemeinschaft (DFG) through Project We 1889/13-1 is gratefully acknowledged.

DATA AVAILABILITY

The data that support the findings of this study are available from the corresponding author upon reasonable request.

REFERENCES

[1]M. Lukosius, J. Dabrowski, J. Kitzmann, O. Fursenko, F. Akhtar, M. Lisker, G. Lippert, S. Schulze, Y. Yamamoto, M. A. Schubert, H. M. Krause, A. Wolff, A. Mai, T. Schroeder, and G. Lupina, ACS Appl. Mater. Interfaces **8**, 33786–33793 (2016).
[2]J.-H. Lee, E. K. Lee, W.-J. Joo, Y. Jang, B.-S. Kim, J. Y. Lim, S.-H. Choi, S. J. Ahn, J. R. Ahn, M.-H. Park, C.-W. Yang, B. L. Choi, S.-W. Hwang, and D. Whang, Science **344**(6181), 286–289 (2014).
[3]I. Pasternak, P. Dabrowski, P. Ciepielewski, V. Kolkovsky, Z. Klusek, J. M. Baranowski, and W. Strupinski, Nanoscale **8**, 11241–11247 (2016).
[4]F. Cavallo, R. R. Delgado, M. M. Kelly, J. R. Sánchez Pérez, D. P. Schroeder, H. G. Xing, M. A. Eriksson, and M. G. Lagally, ACS Nano **8**(10), 10237–10245 (2014).
[5]P. Willke, M. A. Schneider, and M. Wenderoth, Ann. Phys. **529**, 1700003 (2017).
[6]S.-H. Ji, J. B. Hannon, R. M. Tromp, V. Perebeinos, J. Tersoff, and F. M. Ross, Nat. Mater. **11**, 114–119 (2012).
[7]K. W. Clark, X.-G. Zhaned, I. V. Vlassiouk, G. He, R. M. Feenstra, and A.-P. Li, ACS Nano **7**(9), 7956–7966 (2013).
[8]P. Willke, T. Druga, R. G. Ulbrich, M. A. Schneider, and M. Wenderoth, Nat. Commun. **6**, 6399 (2015).
[9]A. Sinterhauf, G. A. Traeger, D. Momeni Pakehi, P. Schädlich, P. Willke, F. Speck, T. Seyller, C. Tegenkamp, K. Pierz, H. W. Schumacher, and M. Wenderoth, Nat. Commun. **11**, 555 (2020).
[10]P. Willke, C. Möhle, A. Sinterhauf, T. Kotzott, H. K. Yu, A. Wodtke, and M. Wenderoth, Carbon **102**, 470–476 (2016).
[11]Y. Yamamoto, P. Zaumseil, T. Arguirov, M. Kittler, and B. Tillack, Solid-State Electron. **60**, 2–6 (2011).
[12]R. Scholz, U. Gösele, E. Niemann, and F. Wischmeyer, Appl. Phys. A **64**, 115–125 (1997).
[13]T. Druga, M. Wenderoth, F. Lüpke, and R. G. Ulbrich, Appl. Phys. Lett **103**, 051601 (2013).
[14]M. Mayer, AIP Conf. Proc. **475**, 541 (1999).
[15]H. Okamoto and T. B. Massalski, Bull. Alloy Phase Diagrams **5**, 592 (1984).
[16]A. Almozouzi, J. Bernardini, E. G. Moya, H. Bracht, N. A. Stolwijk, and H. Mehrer, J. Appl. Phys.. **70**, 1345 (1991).
[17]Y. Gan, L. Sun, and F. Banhart, Small **4**, 587 (2008).
[18]S. Malola, H. Häkkinen, and P. Koskinen, Appl. Phys. Lett. **94**, 043106 (2009).
[19]S. Stolbov and M. Alcántara Ortigoza, J. Chem. Phys. **142**, 154703 (2015).